J. Biophotonics **10**, No. 2, 294–302 (2017) / **DOI** 10.1002/jbio.201500327

Journal of BIOPHOTONICS

FULL ARTICLE

Highly sensitive SERS analysis of the cyclic Arg–Gly–Asp peptide ligands of cells using nanogap antennas

Alejandro Portela[1], *Taka-aki Yano*[1], *Christian Santschi*[2], *Olivier J. F. Martin*[2], *Hitoshi Tabata*[*, 3], *and Masahiko Hara*[*, 1]

[1] Department of Chemical Science and Engineering, Tokyo Institute of Technology, Midori-ku, Yokohama, Kanagawa 226-8502, Japan
[2] Nanophotonics and Metrology Laboratory, Swiss Federal Institute of Technology Lausanne, Lausanne CH-1015, Switzerland
[3] Bioengineering Department, Engineering School, The University of Tokyo, Bunkyo-ku, 113-8656, Tokyo, Japan

Received 15 December 2015, revised 9 March 2016, accepted 6 April 2016
Published online 3 May 2016

Key words: Raman, SERS, fluctuations, cyclic RGD, nanogap antennas, plasmonic, biophotonics

The cyclic RGD (cRGD) peptide ligands of cells have become widely used for treating several cancers. We report a highly sensitive analysis of c(RGDfC) using surface enhanced Raman spectroscopy (SERS) using single dimer nanogap antennas in aqueous environment. Good agreement between characteristic peaks of the SERS and the Raman spectra of bulk c(RGDfC) with its peptide's constituents were observed. The exhibited blinking of the SERS spectra and synchronization of intensity fluctuations, suggest that the SERS spectra acquired from single dimer nanogap antennas was dominated by the spectrum of single to a few molecules. SERS spectra of c(RGDfC) could be used to detect at the nanoscale, the cells' transmembrane proteins binding to its ligand.

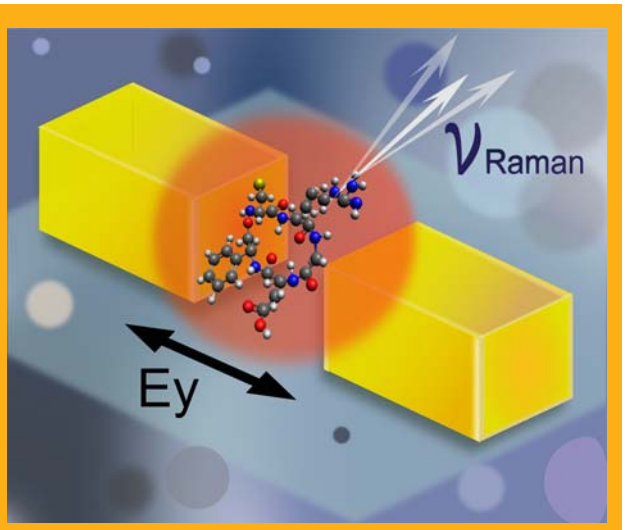

SERS of cyclic RGD on nanogap antenna.

1. Introduction

Understanding the interaction between out-expressed proteins in cancer cells and their extracellular matrix (ECM) represents a key process for improving current cancer therapies and diagnoses. ECM proteins such as fibronectin, vitronectin, and laminin can be substituted by using a small synthetic peptide named RGD (R: arginine (Arg); G: glycine (Gly); D: aspartic acid (Asp)) [1]. This synthetic peptide, in its cyclic conformation, exhibits higher stability toward sterilization, heat treatment, pH-variations, and storage [2]. Several clinical studies involving the use of cyclic (or *cyclo*) RGD (cRGD) for imaging, chemotherapeutic strategies of drug delivery systems are underway [3, 4]. cRGD peptides can

* Corresponding authors: e-mails: masahara@echem.titech.ac.jp; tabata@bioeng.t.u-tokyo.ac.jp

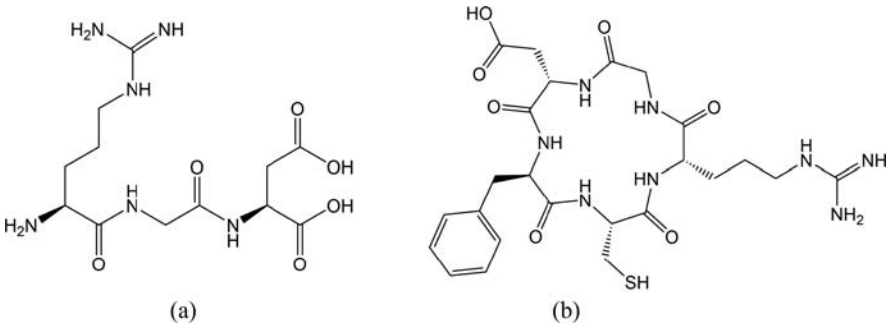

Figure 1 (**a**) Chemical structure of the linear RGD tripeptide molecule in its natural conformation (**b**) the cyclic RGD peptide configuration, c(RGDfC), used in this work.

effectively trigger cell adhesion onto nanostructures that address selective cell lines [5]. Of particular interest, c(RGDfV) exhibited a tenfold stronger binding affinity toward αvβ3 integrin [6]. Figure 1(a) and (b) show the natural structure of the linear RGD and the c(RGDfC) peptides, respectively, where the fourth amino acid is substituted by cysteine (Cys), without loss of affinity [5]. Among all integrins, αvβ3 is likely the most strongly involved in the regulation of angiogenesis; it is widely expressed on blood vessels of human tumor biopsy samples but not on vessels in normal tissues [3]. Integrins mediate adhesive events during various cancer stages such as malignant transformation, invasion, and metastasis [7].

Several spectroscopic methods have been used to investigate the structure of RGD peptides [8]. Vibrational spectroscopy and especially Raman-based spectroscopy methods have recently achieved astonishing results in describing cell biological processes in both in-vitro [9] and *in-vivo* studies [10]. However, traditional Raman spectroscopy is limited by the small amount of scattered photons, which are easily affected by fluorescence or by stronger Rayleigh scattering. Surface enhanced Raman spectroscopy (SERS) has shown an enhancement factor of approximately 10^8 compared to normal Raman cross sections, thanks to the contributions of the electromagnetic (EM) and chemical (CE) enhancement factors [11]. The term "*hot-spots*" is commonly used to describe the high intensity electromagnetic field excited at nanostructures surfaces [12]. They have been reported to conventionally occur on rough metallic surfaces and metallic nanoparticle aggregates; they also occur in plasmonic nanogap antennas [13–15] and in the metallic tip of cantilevers used in a technique called tip-enhanced Raman spectroscopy (TERS) [16].

A nanogap antenna enables nanoscale spatial resolution, leading to more precise spectral analysis than conventional averaged surface enhanced spectra. Dipole nanogap antennas allow fine-tuning of the plasmon resonance condition used for SERS, as was experimentally demonstrated by precisely controlling geometrical parameters such as the gap dimension and the length of the arms [17]. The tunability of the plasmon resonance constitutes a clear advantage of the dipole nanogap antennas compared to colloidal or randomly structured metal-island films. With respect to TERS strategies, the possibility of acquiring signals from different spots almost instantly arises as the most remarkable advantage of the proposed approach. This technique could enable monitoring the local protein binding through the detection of SERS spectral modifications at a single nanogap hot-spot.

The literature contains some reports of Raman signals of linear, modified RGD tripeptides [18, 19] being used to evaluate the adhesion and viability of living cells on biofunctionalized surfaces. In most of these reports, linear RGD peptide chains were used; those that included the cRGD peptide were combined with more complex components, which limits the possibility for elucidating the Raman components specifically related to the RGD molecule [20, 21]. Schultz's group recently reported a novel approach involving the use of TERS to detect the αvβ3 integrin on the top surface of fixed cells on the basis of integrin's bioaffinity with cRGD [22]. However, this approach cannot monitor the interaction between the cRGD and the integrins involved in cell adhesion to the surface, which is also difficult to assess by diffraction-limited immunofluorescence microscopy. Furthermore these authors did not identify or elucidate the origins of the Raman bands of RGD peptide targeting the αvβ3 integrin.

To the best of our knowledge, the literature contains no systematic experimental analysis of the Raman spectroscopic bands of linear or cyclic RGDs. This work reports for first time the SERS spectra, acquired using a single dimer nanogap antenna, of this important biomolecule in an aqueous environment.

A significant segment (~45%) of the cRGD participates in the binding with αvβ3 integrin, causing a distortion of the cRGD upon reaction, as demonstrated in molecular simulation models [23]. Thus, we believe that precise identification of the Raman spectrum of cRGD could provide basic information related to the dynamics and features of nanoscale ligand-receptor binding of the αvβ3 integrins and potentially enable the detection of this reaction only on the basis of the modification of the Raman spectra of a short ligand peptide.

2. Experimental

Nanogap antenna fabrication: Gold nanogap antennas were fabricated on glass substrates using lift-off and electron-beam lithography, as described elsewhere [17]. Different nanogap sizes (15–30 nm) and arm's lengths (40–80 nm) were designed, whereas the width and thickness were kept constant at 40 nm.

Optical setup: A dark-field inverted microscope with an oil–immersion objective (Plapon 60 × O, NA = 1.45 TIRFM, Olympus) was used to illuminate the antennas with a halogen lamp [15]. Nanogap antennas were optically characterized in an aqueous environment to determine the antennas' optimum enhancement for the Raman excitation wavelength. A helium–neon laser at 632.8 nm was used to illuminate the nanostructures, with a spot–size area of approximately 1 μm^2.

Normal Raman spectrum of c(RGDfC): A cyclic pentapeptide c(RGDfC) (Anaspec, US) containing Cys was used for binding to the gold antennas. Different illumination powers and exposure times were evaluated, as detailed in the Supporting Information.

SERS of c(RGDfC) on antennas: c(RGDfC) was immobilized onto the gold surface by covalent bonding via Cys. The samples were incubated in a 170 µM aqueous solution at room temperature for 24 h. Subsequently, the residual unbound c(RGDfC) was removed from the samples by thorough rinsing with pure water. The samples were placed on top of the objective using a piezoelectric positioner for precise location of individual antennas.

3. Results and discussion

Figure 2 shows the Raman spectra of the c(RGDfC) in the spectral region between 400 cm^{-1} and 1800 cm^{-1},which is known as the "fingerprint region" because it contains the principal bands used to identify structural characteristics of biomolecules [24]. The peak frequencies are determined using a Lorentzian peak–fitting function. Table 1 contains the Raman band assignments for the powder c(RGDfC) based on the spectra of the constituent elements of the peptide backbone (i.e. Asp [25, 26], Arg [27], Gly [27, 28]); and those of the other two side–chain components (i.e Cys [29, 30] and phenylalanine (Phe) [27, 29]). Although the fourth amino acids of the peptide chain do not affect the binding of the αvβ3 integrin, these additional elements (i.e Phe and Cys) are responsible for prominent peaks in the Raman spectra of biomolecules.

As indicated in Figure 2, the Raman spectrum contains characteristic bands caused by vibrations of polypeptide structures (amide bond, 1447 cm^{-1}),

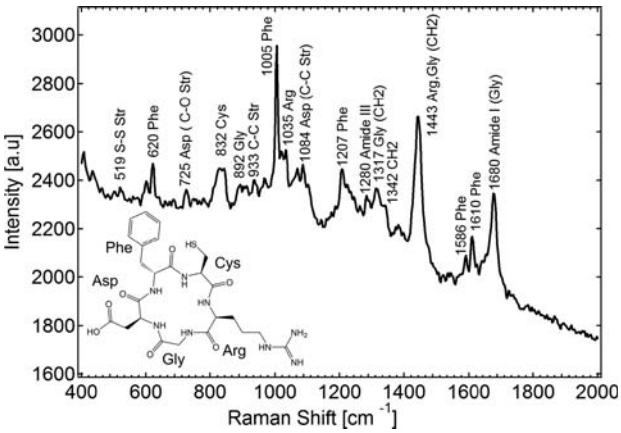

Figure 2 Experimental normal Raman spectrum of c(RGDfC) in the solid powder state, as collected with 1 s exposure. The main components of the Raman bands are assigned on the basis of the Raman bands of the individual constituents (Table 1).

peaks related to the amino acids involved in the integrin binding, and significant peaks originating from the presence of the aromatic amino acid d-Phe (620, 1004, 1210, and 1610 cm^{-1}), in agreement with the results of previous studies on polypeptides analyzed by Raman spectroscopy [31]. A Raman band at 520 cm^{-1} related to a disulfide bridge (S–S) is observed; this band corresponds to the solvated structure of the molecule, consistent with the results of previous Raman studies on proteins containing S–S bonds [24]. A Raman band classified as very strong (1443 cm^{-1}) matches the band previously reported for two of the amino acids, Arg and Gly, and that

Table 1 Experimental normal Raman vibrational spectra of the cyclic RGD peptide c(RGDfC).

Raman [cm^{-1}]	Relative Intensity*	Assignment
519	m	Cysteine (S–S str.)
620	s	Phenylalanine
725	m	Aspartic (C–O str.)
832	br	Cysteine
892	w	Glycine
933	m	C–C str.
1005	vs	Phenylalanine
1035	ms	Arginine
1084	m	Aspartic (C–C str.)
1207	ms	Phenylalanine
1280	m	Amide III
1317	m	Glycine, CH2
1342	w	CH2 defor.
1443	vs	Arginine, glycine, CH2
1586	mw	Phenylalanine
1610	m	Phenylalanine
1680	s	Amide I, glycine

* s, strong; m, medium; w, weak; v, very; br, broad; sh, shoulder; str, stretch; vib, vibration; defor, deformation.

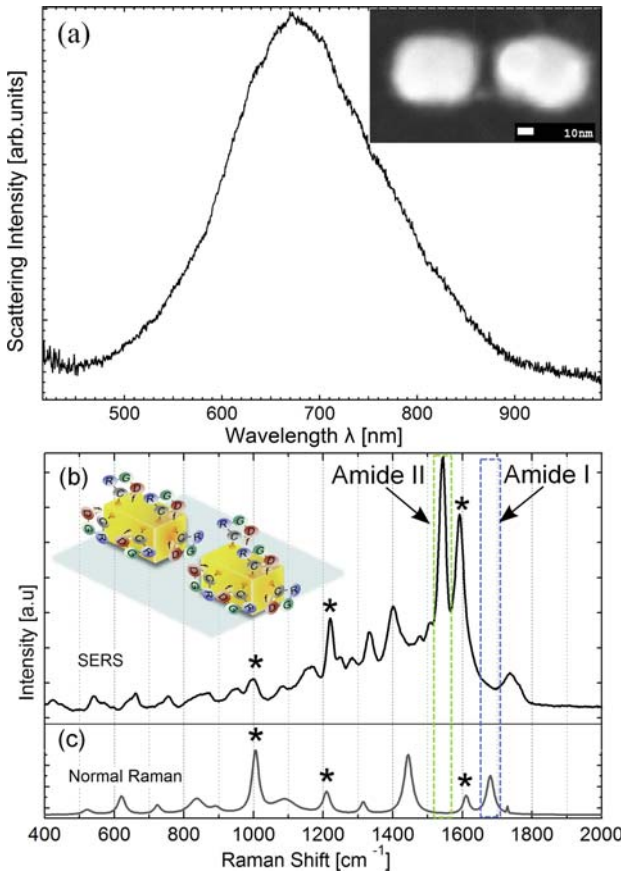

Figure 3 (**a**) Scattering spectrum of a nanogap antenna in an aqueous environment; the inset shows the SEM image for an antenna with an arm length of 60 nm and gap of 15 nm (scale bar: 10 nm). (**b**) Average of five-consecutive SERS spectrum of c(RGDfC) with 1 s exposures. (**c**) Experimental normal Raman spectrum. Asterisks denote the phenyl-ring peaks that match on both the Raman and SERS spectra.

reported for more complex protein structures, where it was assigned to the scissoring of the CH2 bond [32]. Furthermore, no signals associated with possible optically-induced damages of the peptide are observed during the experiment.

SERS of c(RGDfC) on nanogap antennas: SERS spectra from nanogap antennas can provide information about the molecule's conditions on the basis of the highly confined field in the nanogap that defined a potential *hot-spot* for the Raman modes of the c(RGDfC). Figure 3(a) shows the Rayleigh scattering spectrum of a nanogap antenna embedded in an aqueous environment. The spectral region of field enhancement matches the frequency of laser excitation and Raman-scattered light.

The inset in Figure 3(a) shows the scanning electron microscopy (SEM) image of a single gold nanogap antenna. The change on the refractive index due to the binding of the c(RGDfC) peptide on the gold surface led to a red-shift of about 2 nm of the plasmonic resonance. No further changes on plasmon conditions were evident after the SERS experiments on the nanogap antenna, as reported in other experiments [33]. Selective enhancement of SERS modes could be achieved by modifying the refractive index of the surrounding media [34].

Figure 3(b) shows the SERS spectrum of the c(RGDfC) on the nanogap antenna characterized by multiple Raman bands. This spectrum represents the average of five consecutive spectra with 1 s exposure. For comparison, Figure 3(c) shows the normal Raman spectrum of bulk c(RGDfC) after smoothing and fitting of the spectrum shown in Figure 2 using a Lorentzian function. Notably, several peaks are observed in both the normal Raman and the SERS spectrum, confirming the reliability of nanoantennas as a SERS substrate for relatively complex biological molecules. Several dominant Raman bands in the normal spectrum and SERS spectrum of Phe match (i.e., those at ~1002 cm^{-1}, ~1215 cm^{-1}, ~1597 cm^{-1}), with only slight variations, as indicated by the asterisks in both spectra in Figures 3(b) and (c).

Among the bands assigned to Phe, the one at 1595 cm^{-1} exhibits the strongest intensity enhancement. The differences in enhancement between bands of the same molecule have been explained through density functional theory (DFT) calculations; in particular, the orientation of the phenyl ring with respect to the metal surface was observed to cause dramatic changes in the enhanced vibrational modes [35]. We hypothesize that the phenyl ring of the c(RGDfC) peptide is oriented perpendicular to the gold surface, as sketched in Figures 4, facing the nanogap and thereby enhancing the quadrant stretching in-plane vibrational mode of the phenyl ring at 1600 cm^{-1} [36, 37]. This orientation agrees with a previous representation of a similar cyclic RGD polypeptide (RGDfE) found on the Protein Data Bank (PDB, 1FUL) [38] and with another report of a wide set of peptide combinations investigated on silver SERS surfaces [28].

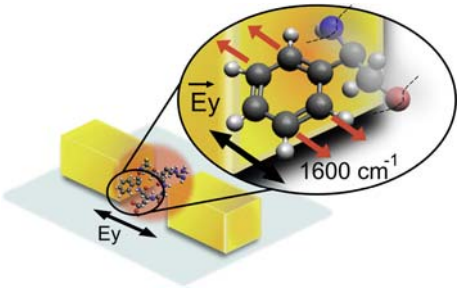

Figure 4 Proposed orientation of the Phe residue of the c(RGDfC) in the nanogap region with respect to the electromagnetic field (Ey) excited on the antenna.

The higher-frequency vibrations exhibit the most significant differences between the normal and SERS spectra. An enhanced SERS peak at 1402 cm^{-1}, presumably from Cys, has been previously associated with the asymmetric stretching vibration of COO^- group [30]. The prominent enhancement of the carboxylate band has been also related to the interaction of COO^- with the metal surface through the π-system of this group [30, 39].

A broad peak with low to medium intensity was also noticeably enhanced in the range from 1736–1764 cm^{-1} in the SERS spectra (Figure 3b). Although this band is not commonly discussed for peptides, it can be assigned as a C=O stretch (1735–1760 cm^{-1}) [36, 40]. It should be mentioned that complete coincidence between the normal Raman and the SERS spectra is not expected for this kind of single structure measurement because the observed large enhancement is partially attributed to chemical enhancement. This implies that the molecule-metal interaction affect, the vibrational modes and, therefore the Raman spectral features [41], as discussed below for the case of amide I/ II.

Amide II enhancement vs Amide I silence: Remarkably, we observed a substantial enhancement of the amide II band (1544 cm^{-1}) [24, 42], which is related to coupled vibrational modes of the peptide bonds. The contrasting increase in the signal intensity for the amide II (N–H bending coupled with C–N stretching) bands with respect to normal Raman spectra has also been reported in TERS and SERS studies [39, 41] and can be interpreted as evidence that c(RGDfC) was not denatured by thermal-induced damages. However, in previous studies of RGD peptides using SERS or TERS, the amide II band was not clearly identified [18, 19, 21, 22].

Conversely, the amide I band which appeared as a high-intensity peak at ~1680 cm^{-1} in the normal Raman spectrum of bulk c(RGDfC), was not observed in the SERS spectrum. This phenomenon of drastic suppression of the amide I band has been referred as the "silence" of amide I [43]. Recently, in an study covering TERS and SERS, researchers approached this effect using different lengths of peptides [44]. They concluded that the silence of the amide I SERS band is sensitive to separations of about 1 nm and occurs when the peptide bond is located at a "bulky distance" from the metal surface.

In our results, we observed an intriguing enhancement of the amide II band associated also with a peptide-bond mode. Thus, in the case of c(RGDfC), we consider that a different vibrational mode of the peptide-bond was enhanced as a result of the molecule's structure modification caused by the interaction with the metal surface. Another possibility is related to the surface selection rules [45] that could determine the orientation of the cyclic segment of the peptide with respect to the EM field excited in the antenna. In particular, this explanation is supported by previous reports [46, 47] wherein the peptide orientation was deduced on the basis of the amide I/amide II dichroic ratio and indicated a perpendicular orientation of the transition moment of these two amide vibrational modes [46]. In summary, these hypotheses imply that the silencing of the amide I band can occur even in cases where the peptide bond is within the range of the charge-transfer (CT) enhancement of the metal surface, although this issue requires further experimental and theoretical investigations.

On the basis of the MM2 classical model of force fields representation [48], we hypothesize that the self-assembly orientation of the c(RGDfC) may predispose the backbone of this cyclic peptide to be oriented parallel to the gold surface of the nanogap a fact supported by the wide range of empirical applications using cRGD for targeting the αvβ3 integrin. Collectively, these evidences suggests that after binding to the gold surface, the RGD sequence remains exposed and is thus well oriented to bind the integrin, which possesses a highly specific binding location (i.e., between the α and β segments), as suggested in the series of papers by Xiong et al. [23, 49].

Temporal intermittency of SERS spectra (blinking): Figure 5(a) shows a waterfall plot with a second-based timescale for the c(RGDfC) spectra on a gold nanogap antenna. High-intensity fluctuations or intermittency of the signal are evident for the sequence shown. The drastic intensity fluctuations, known as "blinking", which results in the on/off switching in the Raman spectra are characteristic of the SERS and TERS when a single molecule (or a small number of molecules) is located at the probing regions under an extremely high electromagnetic field at the nanostructured surface [50–52]. The blinking effect of single-molecule SERS (SM-SERS) is thought to be related to (i) photoinduced ionization of the adsorbed molecule, (ii) reversible activation and quenching of the chemical enhancement, and (iii) thermally induced slow diffusion or desorption of the molecule from the metal surface [12, 50, 53]. The intensity modulation of practically all of the bands confirms the complex temporal variation of the SERS mechanism.

Figure 5(b) shows the overall spectrum (Sum-SERS) of the c(RGDfC) for the region marked with a brace and labelled IV in Figure 5(a). This spectrum corresponds to the average of the SERS individual spectra from 40 s to 44 s, constituting the "bright" state of the molecule. A single spectral line collected at 41 s, as obtained, is represented in Figure 5(b) as III with a graphical offset on the vertical axis. A third trace (II), obtained at 35 s and corresponding to the "dark" state of the molecule, and a

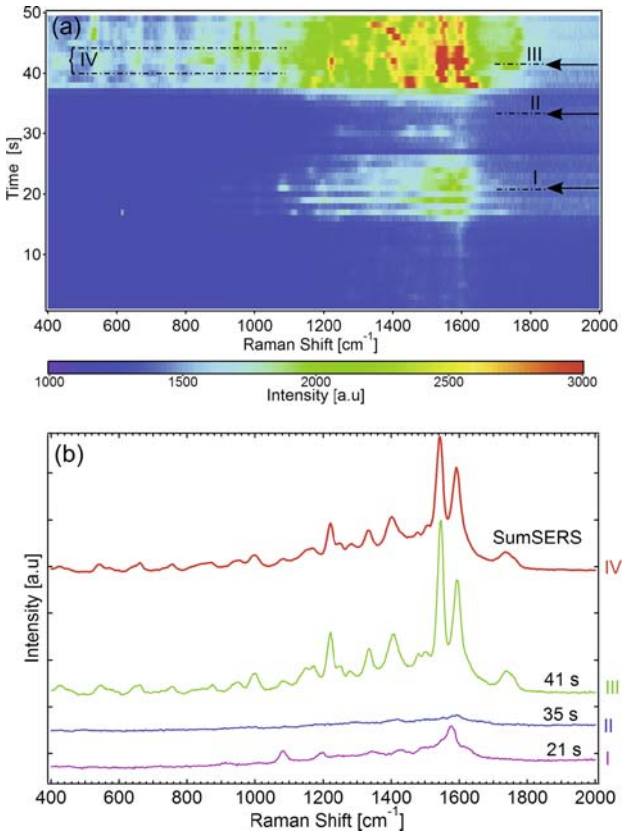

Figure 5 (**a**) Time evolution map of the SERS intensity over 50 spectra. Each line corresponds to an intensity plot of 1 s. The intensity is represented by the color scale; the vertical axis represents the spectrum number, whereas the horizontal axis shows the Raman frequency. (**b**) Representative spectrum of the low-intensity state (I) at 21 s (magenta), dark state (II) at 35 s (blue), the bright state (III) at 41 s (green), and the average of five consecutive spectra from 40 s to 44 s, SumSERS (IV) (red).

fourth trace (I) obtained at 21 s, which represents a low-intensity spectrum corresponding to a transient region at approximately 20 s, are included in Figure 5(b) for reference.

Relative fluctuation of peak position and intensity: In Figure 6(a), although a certain correspondence between sequential spectral lines in the Raman bands is evident, closer observation reveals a substantial fluctuation in both the frequency and intensity of the Raman peaks.

The relative fluctuations, on a 1 s time scale, occur on a time scale faster than the aforementioned blinking effect. Figure 6(a) shows a 10 s sequence, together with the average spectrum (SumSERS, scaled by 2.5). The principal Raman bands (A–H) are indicated in a sequence of 10 representative spectra. The fluctuations do not uniformly modify the SERS spectra, suggesting that their origin is not related to fluctuations in the experimental conditions, but intrinsically related to the plasmonic enhancement, the changes in the vibrational mode of the molecule, or the CE by the interaction with the gold surface.

Figure 6(b) shows the temporal fluctuations of the peak frequencies determined after Lorentzian fitting of each spectrum of the spectra collected between 40 s and 50 s. Spectral lines at 45 s and 48 s were excluded in this figure since bands E and F were not identified and therefore their relative spectral variation could not be estimated. No clear correlation is apparent between the frequency peak fluctuation ($\Delta\omega$) and the spectrum number. The peaks corresponding to Phe (B, C and G in Figure 6(b)) exhibit smaller fluctuation of 8 cm^{-1} to 13 cm^{-1}, whereas the remainder peaks of the c(RGDfC) generally exhibit larger fluctuations, for instance band H ($\Delta\omega_H$ = 28.7 cm^{-1}).

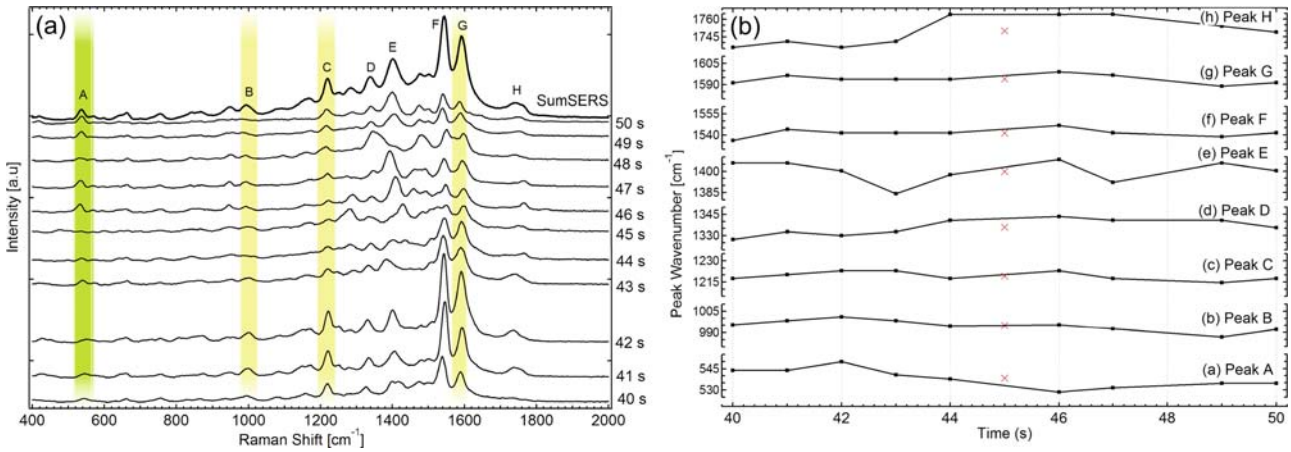

Figure 6 Fluctuation of the SERS spectrum of c(RGDfC). (**a**) Sequence of ten consecutive spectra collected from a nanogap antenna in 1 s time increments and the corresponding average of the signals (SumSERS); three distinctive bands of Phe (B, C, G) are marked with yellow background; a band named A and marked with a green background has not been previously assigned to RGD peptide. (**b**) Temporal fluctuation of the peak positions of the Raman bands (A–H). The value of the corresponding peak in the SumSERS spectrum for the complete segment is indicated with a red mark (×).

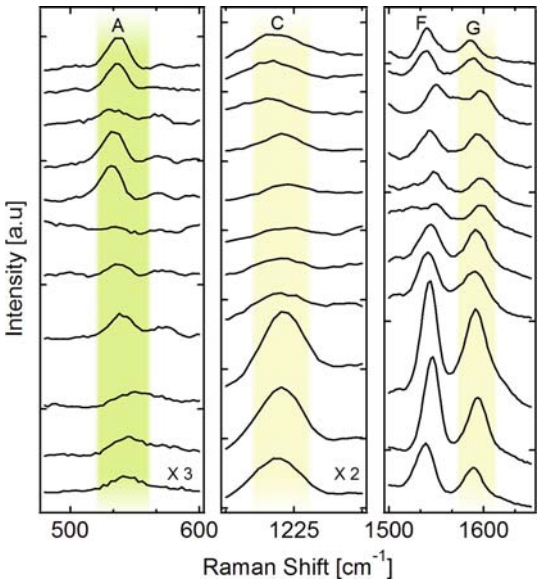

Figure 7 Synchronization of intensity band fluctuations: two intensity-correlated bands from Phe (C = 1215 cm^{-1}, G = 1595 cm^{-1}); and a Raman band showing an anti-correlated synchronization (A = 540 cm^{-1}) with bands C and G.

By contrast, some synchronization of the intensity fluctuation between some Raman bands is evident. Figure 7 summarizes two cases where both correlated and anti-correlated dependences are observed. For instance, the intensities of the Raman bands assigned to Phe (B = 1000 cm^{-1}, C = 1215 cm^{-1}, G = 1593 cm^{-1}) change in unison in almost all spectral lines. Quantitative evaluation of the correlation between pairs of Raman peaks intensity can be assessed through the Pearson correlation coefficient [35]. From Figure 7, the absolute correlation coefficient between the Raman bands C and G (Phe) is +0.93, whereas that between A and G is –0.62, confirming a strong synchronization (correlation and anti-correlation) in the intensity fluctuation of these Raman modes.

The finding of the synchronized fluctuations together with the blinking behavior discussed above endorses that the SERS spectrum of the single nanogap antenna is dominated by a single molecule(s). Because the EM field enhancement was kept constant, there is a consensus that the intensity fluctuations are caused by modification of the CE though the charge transfer (CT) with the metal–ligand interaction [54]. In order to achieve single (or few) molecule sensitivity, the effective Raman scattering cross-section $\sigma^{\mathrm{SERS}}_{\mathrm{Raman\_eff}}$ should be comparable with that of the fluorescence (10^{-17} cm^2). It is defined as $\sigma^{\mathrm{SERS}}_{\mathrm{Raman\_eff}} = \sigma_{\mathrm{Raman}} \cdot G_{\mathrm{EM}} \cdot G_{\mathrm{CE}}$, where G_{EM} and G_{CE} are the electromagnetic and chemical enhancements, respectively, and σ_{Raman} is the normal Raman scattering cross-section of the bulk molecule. Enhancement factor of at least 10^{10} are required to obtain a single molecule sensitivity. Based on our calculations using surface integral equations (SIE), G_{EM} is expected to be $\sim 10^6$, which is in agreement with previous estimates [12, 55]. The G_{EM} can be increased by one to two orders of magnitude when nanofabrication effects due to shape variations [56] and granularity of gold nanorods [57] are taken into account. Thus, for c(RGDfC) adsorbed in the nanogap of the antenna, a G_{CE} of $\sim 10^3$ can be attributed to the chemical mechanism. A previous report of SERS using single bowtie antenna exhibited a G_{CE} of $\sim 10^7$ in order to achieve SM-SERS spectrum [14].

More precise estimation of the G_{CE} using known values of σ_{Raman} of the R6G molecule and rigorous determination of the conversion factor of the optical system has been achieved by Yoshida et al. [58]. However, for the c(RGDfC) used in this work, σ_{Raman} has not yet been determined and, therefore, the value of G_{CE} can only be estimated.

This study is not focused on determining the exact segment of the c(RGDfC) directly enrolled in the CE. However, the SERS analysis suggests a strong interaction of the aromatic ring of the phenyl residue with the gold surface, supported by a remarkable enhancement of the band assigned to the symmetric ring vibrational mode ν8a (Band G 1595 cm^{-1}) considered as indication of an essential role of the CE in the SERS spectra [59, 60]. The mechanism associated with this interaction is explained by the two-state model [61], in particular by the π-back-bonding that enables the Metal-to-Ligand-Charge-Transfer (MLCT) from the highest occupied molecular orbital (HOMO) of the gold atoms to the lowest unoccupied molecular orbital (LUMO) of the molecule.

Interestingly, we found the anti-correlation of the Band G with the band A can be attributed to the change of orientation (and probably to the loss of the interaction with the metal surface) of the phenyl ring. Thus, leading to the correlated decrease of the symmetric in-plane modes corresponding to the bands B, C and G whereas favor the out-of-plane mode of the band A (540 cm^{-1}) that exhibit a lower Raman scattering intensity.

Perspective biological applications of protein binding detection could be affected by the blinking observed in our experiments, which limits the ability to monitor highly dynamics temporal changes of the Raman spectra. However, when a reaction with integrin occur, a remarkable modification of the Raman spectra is expected, as reported in previous works [22, 23], enabling its detection due to the high sensitivity of the dimer nanogap antenna.

On the other hand, although we observed consistent spectra in a number of functionalized nanogap antennas, we found significant variations in frequency/intensity fluctuations. Variations in gap size in antennas with small gaps, caused by imperfections due to nanofabrication issues [15], induce critical variations in the plasmonic resonance position,

which leads to altered G_{EM} for a Raman mode of molecules situated in different antennas. Further improvements have to be achieved in order to implement this method into a robust biological application. Nevertheless, this work demonstrates an original approach for fundamental studies of protein-ligand interactions, while circumventing the problems of large number of Raman bands of complex molecules and the fluctuations, which have been reported to be major limitations for practical applications [37].

4. Conclusion

The Raman spectrum of the cyclic RGD (c(RGDfC)) was presented, and the main Raman bands were identified and assigned on the basis of its amino acid constituents. Good agreement between characteristic peaks of the Raman spectra of the bulk c(RGDfC) and SERS were obtained using a single nanogap antenna. Furthermore, we observed SERS blinking effect that together with synchronized (correlated and anti-correlated) intensity fluctuations between different Raman modes of the phenyl ring are considered indications that the SERS spectra in the dipole nanogap antenna was dominated by a single molecule(s). To achieve single molecule sensitivity, theoretical calculations supports EM enhancement factor of 10^6–10^8, therefore for this dimer nanogap antenna a CE enhancement of at at least 10^3, is expected. These results open the possibility of using gold nanogap antennas as a platform to detect the local binding events of cells, on the basis of the modification of the SERS spectrum corresponding to the c(RGDfC).

Supporting Information

Additional supporting information may be found in the online version of this article at the publisher's website.

Acknowledgements We acknowledge Dr. Shourya Dutta-Gupta for his support on the configuration of the optical setup. This work was supported by Core-to-Core Program, A. Advanced Research Networks from the Japan Society for the Promotion of Science (JSPS).

Author biographies Please see Supporting Information online.

References

[1] M. Pierschbacher, E. G. Hayman, and E. Ruoslahti, Proc. Natl. Acad. Sci. U.S.A. **80**, 1224 (1983).
[2] S. J. Bogdanowich-Knipp, S. Chakrabarti, T. D. Williams, R. K. Dillman, and T. J. Siahaan, J. Pept. Res. **53**, 530 (1999).
[3] F. Danhier, A. Le Breton, and V. Préat, Mol. Pharm. **9**, 2961 (2012).
[4] H.-Q. Yin, F.-L. Bi, and F. Gan, Bioconjug. Chem. **26**, 243 (2015).
[5] U. Hersel, C. Dahmen, and H. Kessler, Biomaterials **24**, 4385 (2003).
[6] M. Pfaff, K. Tangemann, B. Müller, M. Gurrath, G. Müller, H. Kessler, R. Timpl, and J. Engel, J. Biol. Chem. **269**, 20233 (1994).
[7] J. S. Desgrosellier and D. A. Cheresh, Nat. Rev. Cancer **10**, 9 (2010).
[8] J. S. Stevens, A. C. Luca, M. Pelendritis, G. Terenghi, S. Downes, and S. L. M. Schroeder, Surf. Interface Anal. **45**, 1238 (2013).
[9] L. Opilik, T. Schmid, and R. Zenobi, Annu. Rev. Anal. Chem. (Palo Alto. Calif) **6**, 379 (2013).
[10] J. Popp and L. M. Almond, Ex-Vivo and In-Vivo Optical Molecular Pathology (Wiley Online Library, 2014).
[11] J. N. Anker, W. P. Hall, O. Lyandres, N. C. Shah, J. Zhao, and R. P. Van Duyne, Nat. Mater. **7**, 442 (2008).
[12] K. Kneipp, H. Kneipp, I. Itzkan, R. R. Dasari, and M. S. Feld, J. Phys. Condens. Matter **14**, R597 (2002).
[13] P. Mühlschlegel, H.-J. Eisler, O. J. F. Martin, B. Hecht, and D. W. Pohl, Science **308**, 1607 (2005).
[14] D. P. Fromm, A. Sundaramurthy, A. Kinkhabwala, P. J. Schuck, G. S. Kino, and W. E. Moerner, J. Chem. Phys. **124**, (2006).
[15] Z. Weihua, H. Fischer, T. Schmid, R. Zenobi, and O. J. F. Martin, J. Phys. Chem. C **113**, 14672 (2009).
[16] R. M. Stöckle, Y. D. Suh, V. Deckert, and R. Zenobi, Chem. Phys. Lett. **318**, 131 (2000).
[17] A. Portela, T. Yano, C. Santschi, H. Matsui, T. Hayashi, M. Hara, O. J. F. Martin, and H. Tabata, Appl. Phys. Lett. **105**, 91105 (2014).
[18] W. A. El-Said, T. H. Kim, H. Kim, and J. W. Choi, PLoS One **6** (2011).
[19] T. H. Kim, W. A. El-Said, J. H. An, and J. W. Choi, Nanomedicine Nanotechnology, Biol. Med. **9**, 336 (2013).
[20] X. Liu, W. Mo, L. Dai, X. Yan, and H. Song, Protein Pept. Lett. **13**, 47 (2006).
[21] Y. C. Shin, J. H. Lee, L. Jin, M. J. Kim, J.-W. Oh, T. W. Kim, and D.-W. Han, Biomater. Res. **18**, 14 (2014).
[22] H. Wang and Z. D. Schultz, ChemPhysChem **15**, 3944 (2014).
[23] J.-P. Xiong, T. Stehle, R. Zhang, A. Joachimiak, M. Frech, S. L. Goodman, and M. A. Arnaout, Science **296**, 151 (2002).
[24] M. L. De La Chapelle and A. Pucci, Nanoantenna: Plasmon-Enhanced Spectroscopies for Biotechnological Applications (CRC Press, 2013).
[25] J. T. López Navarrete, V. Hernández, and F. J. Ramírez, J. Mol. Struct. **348**, 249 (1995).
[26] J. L. Castro, M. A. Montanez, J. C. Otero, and J. I. Marcos, J. Mol. Struct. **349**, 113 (1995).

[27] J. De Gelder, K. De Gussem, P. Vandenabeele, and L. Moens, J. Raman Spectrosc. **38**, 1133 (2007).
[28] S. Stewart and P. Fredericks, Spectrochim. Acta Part A Mol. Biomol. Spectrosc. **55**, 1641 (1999).
[29] E. Podstawka, Y. Ozaki, and L. M. Proniewicz, Appl. Spectrosc. **59**, 1516 (2005).
[30] G. D. Fleming, J. J. Finnerty, M. Campos-Vallette, F. Celis, A. E. Aliaga, C. Fredes, and R. Koch, J. Raman Spectrosc. **40**, 632 (2009).
[31] R. Tuma, J. Raman Spectrosc. **36**, 307 (2005).
[32] M. Gniadecka, O. Faurskov Nielsen, D. H. Christensen, and H. C. Wulf, J. Invest. Dermatol. **110**, 393 (1998).
[33] T. Itoh, M. Iga, H. Tamaru, K. Yoshida, V. Biju, and M. Ishikawa, J. Chem. Phys. **136**, 024703 (2012).
[34] K. Yoshida, T. Itoh, V. Biju, M. Ishikawa, and Y. Ozaki, Appl. Phys. Lett. **95**, 263014 (2009).
[35] T. Ichimura, H. Watanabe, Y. Morita, P. Verma, S. Kawata, and Y. Inouye, J. Phys. Chem. C **111**, 9460 (2007).
[36] P. J. Larkin, IR and Raman Spectroscopy – Principles and Spectral Interpretation (2011).
[37] E. Smith and G. Dent, Modern Raman Spectroscopy – A Practical Approach (John Wiley & Sons, Ltd, 2005).
[38] N. Assa-Munt, X. Jia, P. Laakkonen, and E. Ruoslahti, Biochemistry **40**, 2373 (2001).
[39] T. Deckert-Gaudig, E. Bailo, and V. Deckert, Phys. Chem. Chem. Phys. **11**, 7360 (2009).
[40] D. Lin-Vien, N. B. Colthup, W. G. Fateley, and J. G. Grasselli, The Handbook of Infrared and Raman Characteristic Frequencies of Organic Molecules (Elsevier, 1991).
[41] E. Podstawka, Y. Ozaki, and L. M. Proniewicz, Appl. Spectrosc. **58**, 570 (2004).
[42] G. Socrates, Infrared and Raman Characteristic Group Frequencies (2004).
[43] E. Podstawka and Y. Ozaki, Biopolymers **89**, 941 (2008).
[44] D. Kurouski, T. Postiglione, T. Deckert-Gaudig, V. Deckert, and I. K. Lednev, Analyst **138**, 1665 (2013).
[45] M. Moskovits, J. Chem. Phys. **77**, 4408 (1982).
[46] T. Miyazawa and E. R. Blout, J. Am. Chem. Soc. **83**, 712 (1961).
[47] H. S. Kim, J. D. Hartgerink, and M. R. Ghadiri, J. Am. Chem. Soc. **120**, 4417 (1998).
[48] N. L. Allinger, J. Am. Chem. Soc. **99**, 8127 (1977).
[49] J.-P. Xiong, T. Stehle, B. Diefenbach, R. Zhang, R. Dunker, D. L. Scott, A. Joachimiak, S. L. Goodman, and M. A. Arnaout, Science (80) **294**, 339 (2001).
[50] J. T. Krug, G. D. Wang, S. R. Emory, and S. Nie, J. Am. Chem. Soc. **121**, 9208 (1999).
[51] A. Otto, J. Raman Spectrosc. **33**, 593 (2002).
[52] P. G. Etchegoin, M. Meyer, E. Blackie, and E. C. Le Ru, Anal. Chem. **79**, 8411 (2007).
[53] Y. Maruyama and M. Futamata, J. Raman Spectrosc. **36**, 581 (2005).
[54] N. Valley, N. Greeneltch, R. P. Van Duyne, and G. C. Schatz, J. Phys. Chem. Lett. **4**, 2599 (2013).
[55] P. Biagioni, J.-S. Huang, and B. Hecht, Rep. Prog. Phys. **75**, 024402 (2012).
[56] A. M. Kern and O. J. F. Martin, Nano Lett. **11**, 482 (2011).
[57] P. Dawson, J. A. Duenas, M. G. Boyle, M. D. Doherty, S. E. J. Bell, A. M. Kern, O. J. F. Martin, A.-S. Teh, K. B. K. Teo, and W. I. Milne, Nano Lett. **11**, 365 (2011).
[58] K. Yoshida, T. Itoh, H. Tamaru, V. Biju, M. Ishikawa, and Y. Ozaki, Phys. Rev. B **81**, 115406 (2010).
[59] J. Castro, M. López Ramírez, I. López Tocón, and J. Otero, J. Colloid Interface Sci. **263**, 357 (2003).
[60] E. Podstawka, R. Borszowska, M. Grabowska, M. Drag, P. Kafarski, and L. M. Proniewicz, Surf. Sci. **599**, 207 (2005).
[61] S. M. Morton and L. Jensen, J. Am. Chem. Soc. **131**, 4090 (2009).